AGU PUBLICATIONS

JGR

Journal of Geophysical Research: Space Physics

RESEARCH ARTICLE

10.1002/2014JA020668

Special Section:
Origins and Properties of Kappa Distributions

The interplay of Kappa and core populations in the solar wind: Electromagnetic electron cyclotron instability

M. Lazar[1,2], S. Poedts[1], and R. Schlickeiser[2]

[1]Center for Plasma Astrophysics, Leuven, Belgium, [2]Institut für Theoretische Physik, Lehrstuhl IV: Weltraum- und Astrophysik, Ruhr-Universität, Bochum, Germany

Key Points:
- Kappa models facilitate realistic predictions in space plasma
- The first formalism assuming both the core and halo temperatures are anisotropic
- The interplay of the Kappa and core populations unveiled in the EMEC instability

Correspondence to:
M. Lazar,
mlazar@tp4.rub.de

Citation:
Lazar, M., S. Poedts, and R. Schlickeiser (2014), The interplay of Kappa and core populations in the solar wind: Electromagnetic electron cyclotron instability, *J. Geophys. Res. Space Physics*, *119*, 9395–9406, doi:10.1002/2014JA020668.

Received 27 SEP 2014
Accepted 14 NOV 2014
Accepted article online 9 DEC 2014
Published online 18 DEC 2014

Abstract Recently, a realistic parameterization was proposed for the kinetic anisotropy and the resulting instabilities in the solar wind plasma. This parameterization is based on observations of the particle velocity distribution, which always comprises a Maxwellian population at low energies, viz. the core, and a suprathermal halo in the tail of the distribution which is best described by the Kappa (power law) models. The cyclotron instability, driven by an anisotropic electron halo, was found to be inhibited by the finite thermal spread in the core, and this effect is highly dependent on the halo-core relative density. In this paper, the interplay between the Kappa and Maxwellian populations is further investigated for more complex (less idealized) situations when both the core and halo temperatures are anisotropic. Growth of this instability is markedly stimulated by the core anisotropy. The wave numbers that are stable for an isotropic core become unstable even for small anisotropies of this population. Just a modest increase of the core anisotropy from $A_c = T_\perp/T_\parallel = 1.2$ to 2 causes the growth rates to enhance by 1 order of magnitude, and the range of unstable wave numbers to extend considerably. When the anisotropies in the core and halo are comparable, the growth rate exhibits two distinct peaks, the first driven by the halo at lower wave numbers and the second driven by the core. However, the first peak is inhibited by the suprathermal populations, while the second peak is sustained, suggesting a more intricate connection between the core and Kappa populations.

1. Introduction

Two of the most important properties of a plasma are dispersion of the fluctuations and their stability. To describe these properties in the solar wind plasma, which is poor collisional, we need information about the energetic distributions of plasma particles. This information is now available from an extensive number of space missions. Thus, for all species of particles in space plasmas, the velocity distribution functions (VDFs) exhibit high-energy (suprathermal) tails which are well fitted by the Kappa power laws, and at lower energies, the core component is well described by a standard Maxwellian [*Maksimovic et al.*, 2005; *Stverak et al.*, 2008; *Pierrard and Lazar*, 2010]. The Kappa distribution function was first proposed as a model for the distributions of electrons observed in magnetosphere [*Vasyliunas*, 1968] and the solar wind at 1 AU [*Scudder and Olbert*, 1979]. For protons and heavier ions, later observational studies have also shown that distributions exhibit suprathermal tails well fitted by the Kappa power laws [*Christon et al.*, 1988, 1991; *Collier et al.*, 1996].

Despite this observational evidence, in the existing attempts to parameterize these distributions, especially the anisotropic distributions and the resulting plasma wave instabilities, only simplified (idealized) models are invoked, which either ignore the suprathermal halo or just minimize the role of the core assuming it cold. There is an additional compromise to incorporate the core with a finite thermal spread in a single, global Kappa that is nearly Maxwellian at low speeds and decreases smoothly as a power law at high speeds. But a single Kappa seems to couple in an artificial, unrealistic way the core and halo components (which otherwise appear to be two distinct components with different origins) and cannot provide a fit as good as a Maxwellian-Kappa combination.

Simplified models imply a reduced number of plasma parameters and are convenient computationally, but they omit important kinetic effects of the plasma particles. For instance, we cannot ignore the halo, which is more anisotropic and can trigger the instability, neither the thermal spread in the core. The core is hot enough even at large heliocentric distances $R > 1$ AU, where the *Ulysses* observations indicate that kinetic energies of the core and halo populations can easily reach comparable levels [*Lazar et al.*, 2015].

The simplest way to build a realistic model is to combine a Maxwellian for the core and one or more Kappas for the suprathermal components, including the halo and the strahls. Such complex models are preferred only in the attempts to describe accurately the observed VDFs [*Maksimovic et al.*, 2005; *Stverak et al.*, 2008], but to deal with them in theoretical predictions is not straightforward. The large number of parameters, especially in the presence of kinetic anisotropies, makes it difficult to identify the instability conditions.

Recently, *Lazar et al.* [2015] have proposed to approach these realistic models starting from simple cases of nonstreaming distributions with isotropic cores, i.e., isotropic temperature $T_{c,\parallel} = T_{c,\perp}$, but anisotropic halos, i.e., anisotropic temperature $T_{h,\parallel} \neq T_{h,\perp}$ (where $\parallel$ and $\perp$ denote directions parallel and perpendicular, respectively, to the magnetic field). Such a model has been found relevant for the slow wind conditions, when the flow speed is sufficiently small ($V_{SW} < 360$ km s^{-1}), and, in general, in the solar wind at sufficiently large heliocentric distances (> 1 AU), when the field-aligned strahl is less pronounced and can be neglected. A comparative study with the cold-core-based model was performed on the instability conditions of the electromagnetic electron cyclotron (EMEC) modes. These modes can result from a decay of the large-scale fluctuations (being responsible for the wave energy dissipation at small scales), but locally, they can also be sustained and amplified by an excess of electron temperature in perpendicular direction ($T_\perp > T_\parallel$). If only driven by the halo anisotropy, the EMEC instability was found to be inhibited by the thermal spread of the core, and this effect is highly dependent on the halo-core relative density and the presence of suprathermal populations (quantified by the power index kappa).

Here we take these results as a guide and extend the approach to more complex situations, when both the core and halo temperatures are anisotropic, i.e., $T_{c,\parallel} \neq T_{c,\perp}$, $T_{h,\parallel} \neq T_{h,\perp}$. Such situations are less idealized and are probably the most encountered in the solar wind [*Marsch*, 2006; *Stverak et al.*, 2008; *Bale et al.*, 2009]. To keep the analysis transparent, we continue to restrict to the solar wind conditions when the strahl component is not significant. After 1 AU, the density of the strahl population is markedly diminished by comparison to the halo population [*Maksimovic et al.*, 2005], and the two-component core-halo model may be sufficient to describe the VDFs. We use the observational data from a survey of slow wind events identified by *Ulysses* between 1995 and 2004. These intervals of slow wind are specified in Table 1 from *Lazar et al.* [2015] and cover a wide range of heliocentric distances, i.e., 1.34 AU $\leqslant R \leqslant$ 5.41 AU and heliolatitudes, $-80° \leqslant$ L $\leqslant +58°$. In the next section, we build the anisotropic models for the Maxwellian and Kappa populations, and based on a qualitative analysis of the observational data, we assign the most relevant cases of temperature anisotropy. Cumulative effects of the anisotropic populations are unveiled in section 3 for the instability of EMEC modes. The influence of suprathermal populations is also shown in our comparative study. The last section summarizes the main results of this study and their implications.

2. Model of Velocity Distribution

The distributions provided by the in situ measurements in the solar wind are fluxes of particles transformed into the frame of bulk flow, such that measurements in the solar wind with sufficiently low speeds present only a dual core-halo structure and no other additional strahl (or streaming) component (see Figures 1 and 2). Here we consider a nonstreaming model relevant for such situations in the solar wind, when the bulk speed is sufficiently low, i.e., $V_{SW} < 360$ km s^{-1}, and the relative density of the strahl is negligibly small $n_s < n_h < n_c$. This model includes distinctively all plasma species, i.e., electrons (denoted by subscript $a = e$), protons (subscript $a = p$), and, eventually, a minor population of heavier ions (subscript $a = i$), as well as their main components, namely, the core (subscript c) and the halo (subscript h)

$$f(v_\parallel, v_\perp) = \sum_{a=e,p,i} \left[f_{a,c}(v_\parallel, v_\perp) + f_{a,h}(v_\parallel, v_\perp) \right]. \tag{1}$$

Each component is assumed gyrotropic (the temperature anisotropy in the plane transverse to the magnetic field is usually less significant) with a biaxis temperature anisotropy $T_\perp \neq T_\parallel$ in polar coordinates $(v_\perp \cos\phi, v_\perp \sin\phi, v_\parallel) = (v_x, v_y, v_z)$. The core is described by a bi-Maxwellian

$$f_c(v_\parallel, v_\perp) = \frac{n_c}{\pi^{3/2} w_\parallel w_\perp^2} \exp\left(-\frac{v_\parallel^2}{w_\parallel^2} - \frac{v_\perp^2}{w_\perp^2} \right), \tag{2}$$

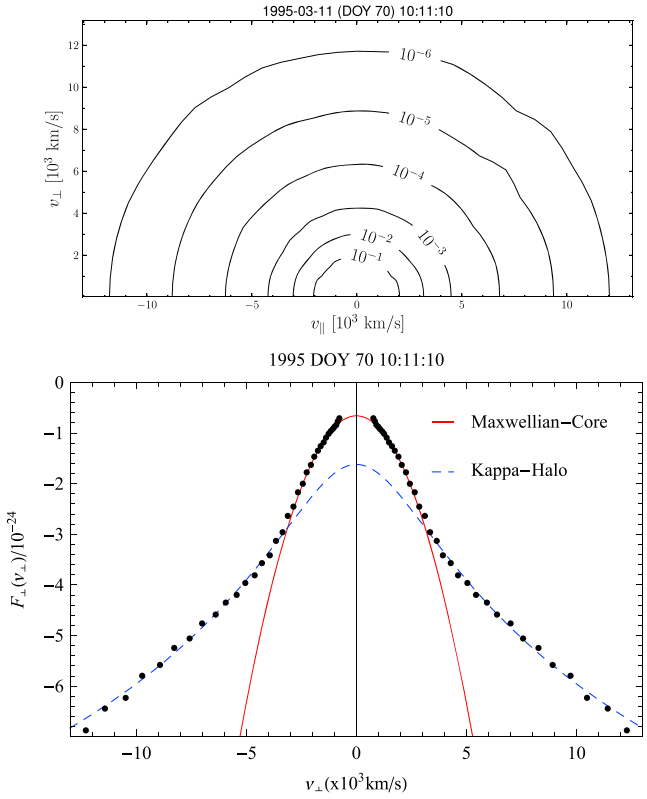

Figure 1. Example of isotropic velocity distribution in the slow wind. (top) Contours of the distribution. (bottom) Perpendicular cut (dots) is fitted with a Maxwellian for the core (solid line) and a Kappa for the halo (dashed line).

and the halo by a bi-Kappa

$$f_h(v_\parallel, v_\perp) = \frac{n_h}{\pi^{3/2}\theta_{h,\parallel}\theta_{h,\perp}^2}\frac{\Gamma[\kappa]}{\kappa^{1/2}\Gamma[\kappa-1/2]}\left(1+\frac{v_\parallel^2}{\kappa\theta_{h,\parallel}^2}+\frac{v_\perp^2}{\kappa\theta_{h,\perp}^2}\right)^{-\kappa-1}, \quad (3)$$

where n_c and n_h are the number densities of these two components and $w_{\parallel,\perp}$ and $\theta_{\parallel,\perp}$ are thermal velocities defined by the temperatures as moments of second order

$$\frac{2k_BT_{c,\parallel}}{m} \equiv 2\int d\mathbf{v}v_\parallel^2 f_c(v_\parallel, v_\perp) = w_\parallel^2, \quad (4)$$

$$\frac{2k_BT_{c,\perp}}{m} \equiv \int d\mathbf{v}v_\perp^2 f_c(v_\parallel, v_\perp) = w_\perp^2, \quad (5)$$

$$\frac{2k_BT_{h,\parallel}}{m} \equiv 2\int d\mathbf{v}v_\parallel^2 f_h(v_\parallel, v_\perp) = \frac{\kappa\theta_{h,\parallel}^2}{\kappa-3/2}, \quad (6)$$

$$\frac{2k_BT_{h,\perp}}{m} \equiv \int d\mathbf{v}v_\perp^2 f_h(v_\parallel, v_\perp) = \frac{\kappa\theta_{h,\perp}^2}{\kappa-3/2}. \quad (7)$$

The bi-Kappa reduces to a bi-Maxwellian in the limit of a very large $\kappa \to \infty$. A particularly simplifying situation is that of *isotropic* distributions (see the example in Figure 1)

$$f_a(v) = f_{a,c}(v) + f_{a,h}(v), \quad (8)$$

when the core is well described by an isotropic Maxwellian, i.e., $w_\parallel = w_\perp = w$ in equation (2), and the halo by an isotropic Kappa, i.e., $\theta_{h,\parallel} = \theta_{h,\perp} = \theta_h$ in equation (3).

Otherwise, both the core and halo components can be anisotropic, in a sense that each can show temperature anisotropy with respect to the magnetic field (see the examples in Figure 2). The case when only the core is anisotropic ($T_{c,\parallel} \neq T_{c,\perp}$) and the halo is isotropic ($T_{h,\parallel} = T_{h,\perp} = T_h$) seems to be unrealistic (not reported by the observations) and is not treated here. The opposite scenario when the core is isotropic ($T_{c,\parallel} = T_{c,\perp} = T_c$), or, at least, less anisotropic than the halo, is more realistic and was analyzed by *Lazar et al.* [2015]. To describe the more complex conditions when both the core and halo components are anisotropic, we consider the same set of slow wind intervals from Table 1 in *Lazar et al.* [2015]. The excess of temperature is predominantly found to manifest in the same direction for both the core and halo components, either in the parallel direction, i.e., $T_{c,\parallel} > T_{c,\perp}$ and $T_{h,\parallel} > T_{h,\perp}$ (see the case in Figure 2 (left)), or in the perpendicular direction, i.e., $T_{c,\parallel} < T_{c,\perp}$ and $T_{h,\parallel} < T_{h,\perp}$ (see Figure 2 (right)). The other combinations are not impossible but are less frequent in this survey. An observational analysis will be published elsewhere with estimates of the temperature anisotropy in the core and halo populations. The question of interest for the present study is only the observational relevance of these anisotropies, and this is summarized in Table 1.

3. Electron Whistler-Cyclotron Modes

In this section we investigate the interplay of the core and halo populations when the anisotropic plasma model in equations (1)–(3) satisfies the instability conditions for the electromagnetic (EM) electron cyclotron

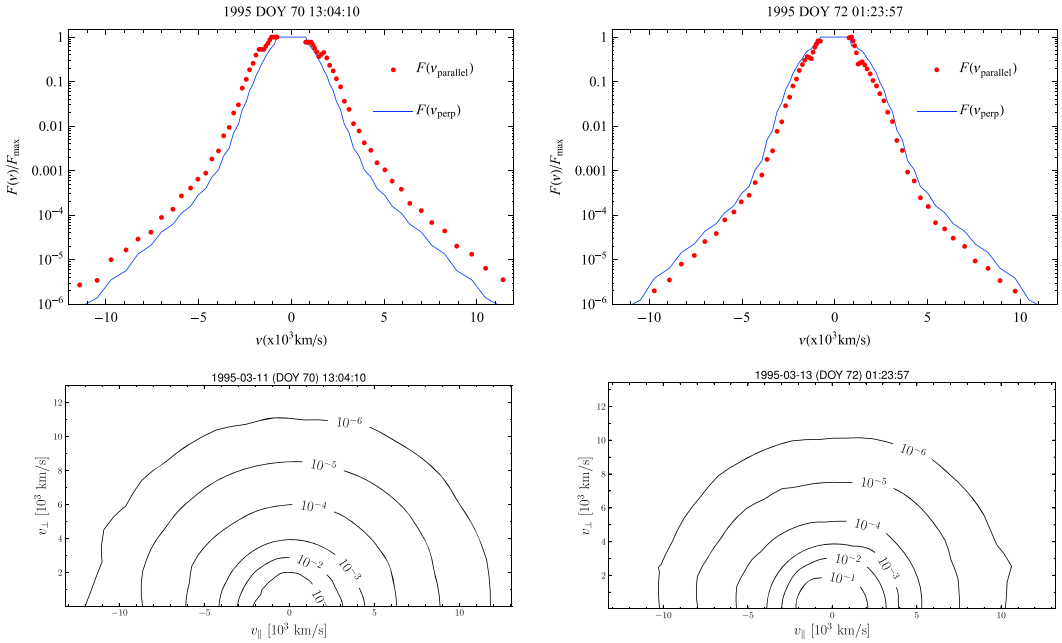

Figure 2. Examples of velocity distributions with temperature anisotropies ($T_{\parallel} \neq T_{\perp}$) in the slow wind. (left) $T_{\parallel} > T_{\perp}$. (right) $T_{\parallel} < T_{\perp}$.

(EMEC) modes. The EM modes propagating parallel to the uniform magnetic field are described by the general dispersion relation (see textbooks by *Gary* [1993] and *Schlickeiser* [2002])

$$\frac{k^2c^2}{\omega^2} = 1 + \frac{4\pi^2}{\omega^2}\sum_{a=e,p,i}\frac{e_a}{m_a}\int_{-\infty}^{\infty}\frac{\mathrm{d}v_{\parallel}}{\omega - kv_{\parallel} \pm \Omega_a}\int_0^{\infty}\mathrm{d}v_{\perp}v_{\perp}^2\left[(\omega - kv_{\parallel})\frac{\partial f_a}{\partial v_{\perp}} + kv_{\perp}\frac{\partial f_a}{\partial v_{\parallel}}\right], \tag{9}$$

where ω and k are, respectively, the frequency and the wave number of the plasma modes, c is the speed of light in vacuum, $\Omega_a = q_aB_0/(m_ac)$ is the (nonrelativistic) gyrofrequency for the particles of sort a, and "$\pm$" is used to distinguish between the circularly polarized electromagnetic modes with right-hand (RH) and left-hand polarizations, respectively. In parallel direction, the EMEC modes are decoupled from electrostatic oscillations and are RH polarized. The instability of these modes is faster than oblique directions [*Kennel and Petschek*, 1966]. Because of their high frequency, these modes interact only with electrons, ions are just immobile, and their contribution can be neglected. In this case we can omit the subscript e. Assuming electrons distributed after a two-component model in (1)–(3), the dispersion relation (9) becomes

$$\frac{k^2c^2 - \omega^2}{\omega_h^2} = \frac{\omega_c^2}{\omega_h^2}\left[A_c - 1 + \frac{A_c(\omega - \Omega) + \Omega}{kw_{\parallel}}Z\left(\frac{\omega - \Omega}{kw_{\parallel}}\right)\right] + A_h - 1 + \frac{A_h(\omega - \Omega) + \Omega}{k\theta_{\parallel}}Z_{\kappa}\left(\frac{\omega - \Omega}{k\theta_{\parallel}}\right), \tag{10}$$

Table 1. Models of Nonstreaming Distributions in the Solar Wind

Number	Microstate	Maxwellian Core	Kappa Halo	Observational Relevance
1	Isotropic	$T_{c,\parallel} = T_{c,\perp} = T_c$	$T_{h,\parallel} = T_{h,\perp} = T_h$	slow wind
2	Anisotropic	$T_{c,\parallel} = T_{c,\perp} = T_c$	$T_{h,\parallel} \neq T_{h,\perp}$	slow wind
3	Anisotropic	$T_{c,\parallel} \neq T_{c,\perp}$	$T_{h,\parallel} = T_{h,\perp} = T_h$	rare/unrealistic
4	Anisotropic	$T_{c,\parallel} \gtrless T_{c,\perp}$	$T_{h,\parallel} \gtrless T_{h,\perp}$	slow wind
5	Anisotropic	$T_{c,\parallel} \gtrless T_{c,\perp}$	$T_{h,\parallel} \lessgtr T_{h,\perp}$	rare

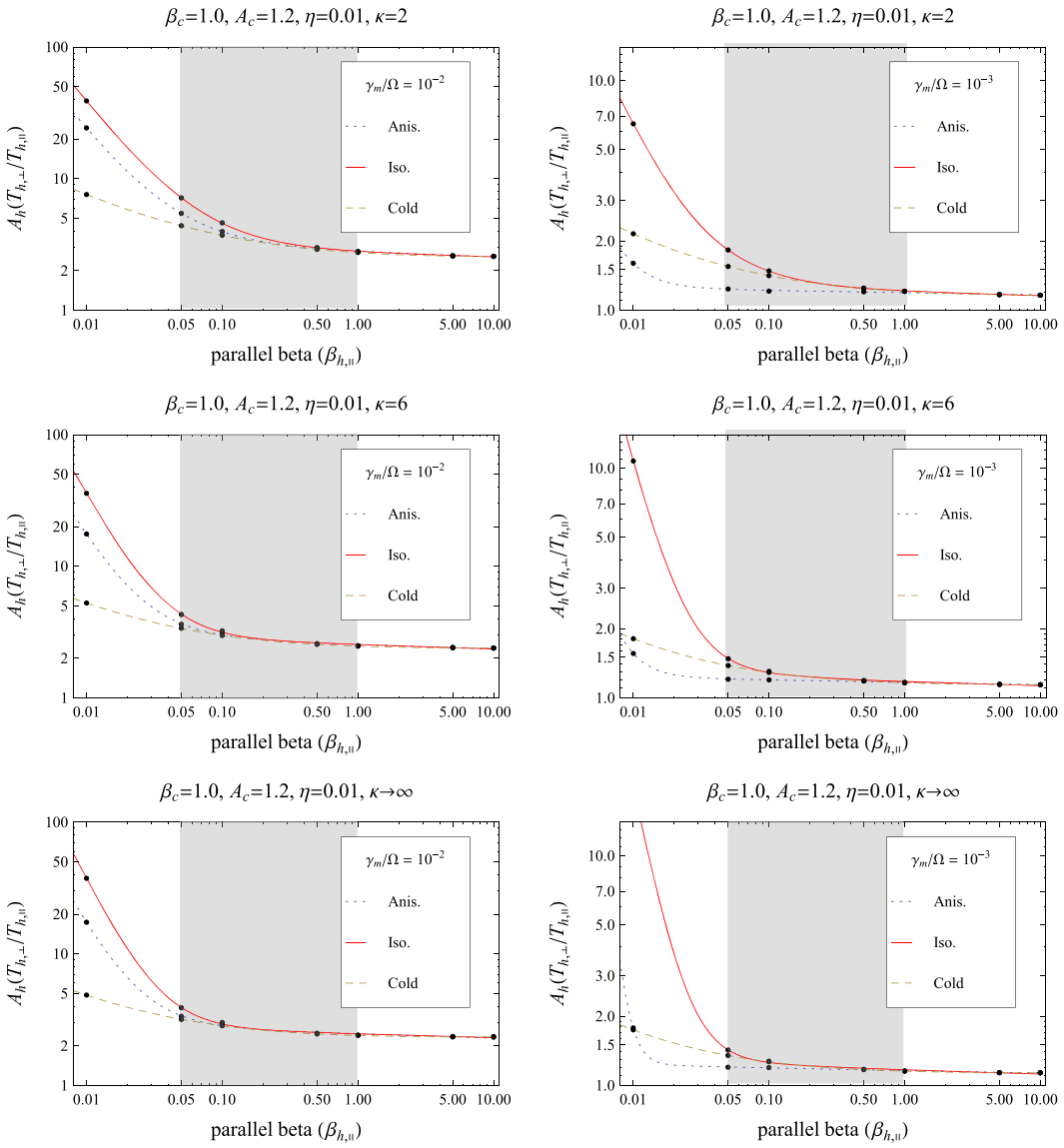

Figure 3. (left) Thresholds $\gamma_m/|\Omega_e| = 10^{-2}$ of the EMEC instability for different models of the distribution function: anisotropic core with $A_c = 1.2$ (dotted lines); isotropic core (solid lines); cold core (dashed lines); and for the Kappa model of the halo (top) $\kappa = 2$, (middle) $\kappa = 6$, and (bottom) $\kappa \to \infty$. (right) The same but for $\gamma_m/|\Omega_e| = 10^{-3}$.

where $\Omega = |\Omega_e|, \omega_{c,h} = (4\pi n_c e^2/m)^{1/2}$ are the plasma frequencies for the core (subscript c) and halo (subscript h) components, $A_{c,h} = (T_\perp/T_\parallel)_{c,h}$ are the temperature anisotropies,

$$Z(f) = \frac{1}{\pi^{1/2}} \int_{-\infty}^{+\infty} dx \, \frac{\exp(-x^2)}{x - f}, \quad \Im(f) > 0, \tag{11}$$

is the Maxwellian plasma dispersion function [*Fried and Conte*, 1961] of argument

$$f = \frac{\omega - \Omega}{k w_\parallel}, \tag{12}$$

and

$$Z_\kappa(f) = \frac{1}{\pi^{1/2}\kappa^{1/2}} \frac{\Gamma(\kappa)}{\Gamma\left(\kappa - \frac{1}{2}\right)} \int_{-\infty}^{\infty} dx \, \frac{(1 + x^2/\kappa)^{-\kappa}}{x - f}, \quad \Im(f) > 0 \tag{13}$$

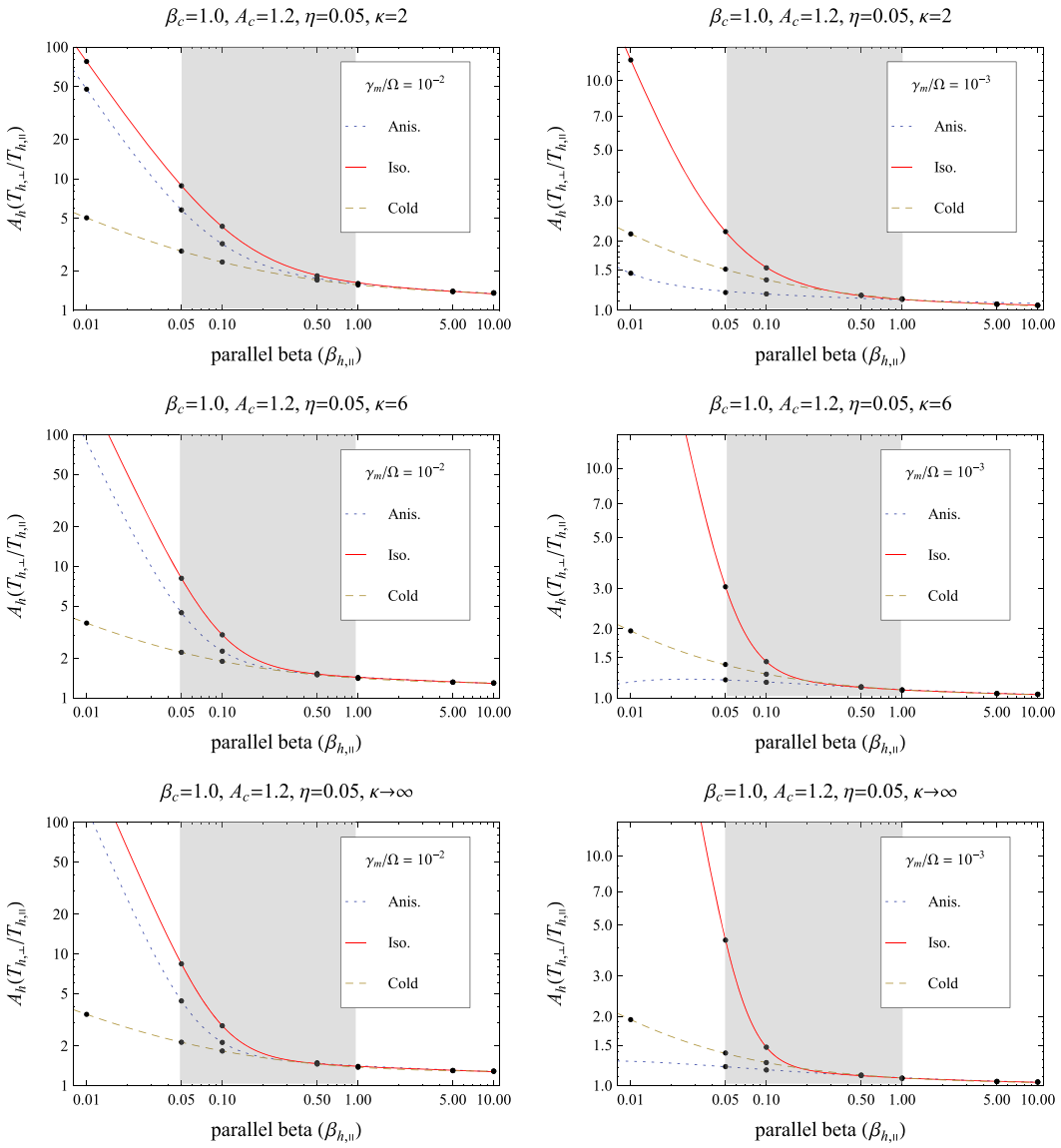

Figure 4. The same as in Figure 3 but for $\eta = 0.05$. (right) The same but for $\gamma_m/|\Omega_e| = 10^{-3}$.

is the Kappa plasma dispersion function [*Lazar et al.*, 2008] of argument

$$f_\kappa = \frac{\omega - \Omega}{k\theta_\parallel}. \tag{14}$$

First, a comparison can be made with the recent results in *Lazar et al.* [2015], where the core was assumed isotropic, i.e., $A_c = 1$, and the dispersion relation reduces to

$$\frac{k^2c^2 - \omega^2}{\omega_h^2} = \frac{\omega_c^2}{\omega_h^2}\frac{\omega}{kw_\parallel} Z\left(\frac{\omega - \Omega}{kw_\parallel}\right) + A_h - 1 + \frac{A_h(\omega - \Omega) + \Omega}{k\theta_\parallel} Z_\kappa\left(\frac{\omega - \Omega}{k\theta_\parallel}\right). \tag{15}$$

Moreover, to compare with the idealized models which completely neglect the thermal spread in the core, i.e., $T_c \to 0$, in equation (15) we can adopt the zero-order approximation for the plasma dispersion function $Z(|f| \gg 1) \simeq -f^{-1}$ in the limit of very large arguments. In this case the dispersion relation becomes

$$\frac{k^2c^2 - \omega^2}{\omega_h^2} = \frac{\omega_c^2}{\omega_h^2(1 - \Omega/\omega)} + A_h - 1 + \frac{A_h(\omega - \Omega) + \Omega}{k\theta_\parallel} Z_\kappa\left(\frac{\omega - \Omega}{k\theta_\parallel}\right). \tag{16}$$

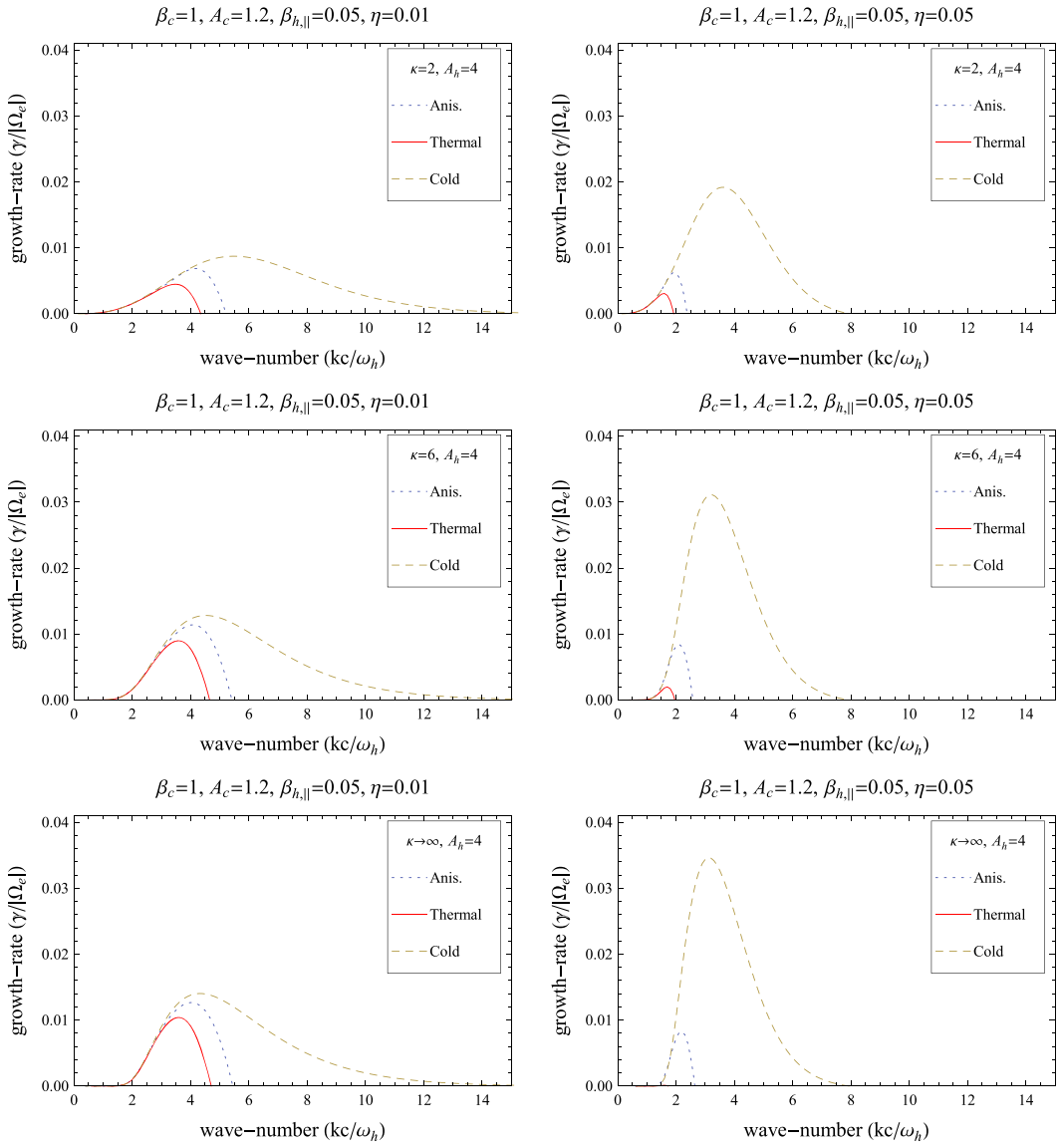

Figure 5. Growth rates of the EMEC instability as provided by our models with a cold core (dashed lines), an isotropic core (solid lines) with $\beta_c = 1$, and an anisotropic core with $\beta_c = 1$ and $A_c = 1.2$. Comparison is extended for two relative densities, (left) $\eta = 0.01$ and (right) $\eta = 0.05$, and three Kappa models with the same $\beta_{h,||} = 0.05$ and $A_h = 4$ but different (top) $\kappa = 2$, (middle) $\kappa = 6$, and (bottom) $\kappa \to \infty$.

Since the EMEC instability is driven by an excess of temperature in perpendicular direction ($T_\perp > T_\parallel$), only the realistic cases numbered with 2 and 4 in Table 1 will be of interest for our analysis.

3.1. Instability Thresholds

The instability thresholds are calculated numerically in order to avoid analytical restrictions introduced by the approximations of the plasma dispersion function in the limits of very small or very large arguments. To enable comparison with the previous models [*Lazar et al.*, 2015], only the parameters describing the Kappa (halo) population are allowed to change and constrain the instability thresholds, and the core parameters are taken fixed. For the range of these parameters, we invoke the observational estimates provided by *Lazar et al.* [2015] for the slow wind events. The same authors proposed a refined form of the inverse correlation law between the temperature anisotropy and the plasma beta (including the second-order term) (see equation (20)), and this form is applied here to find the best fit for the anisotropy thresholds.

The anisotropy thresholds displayed in Figures 3 and 4 are derived for two levels of maximum growth rates $\gamma_m/\Omega = 10^{-2}$ and 10^{-3}, and for three different models of VDFs: (i) both the core and halo components are

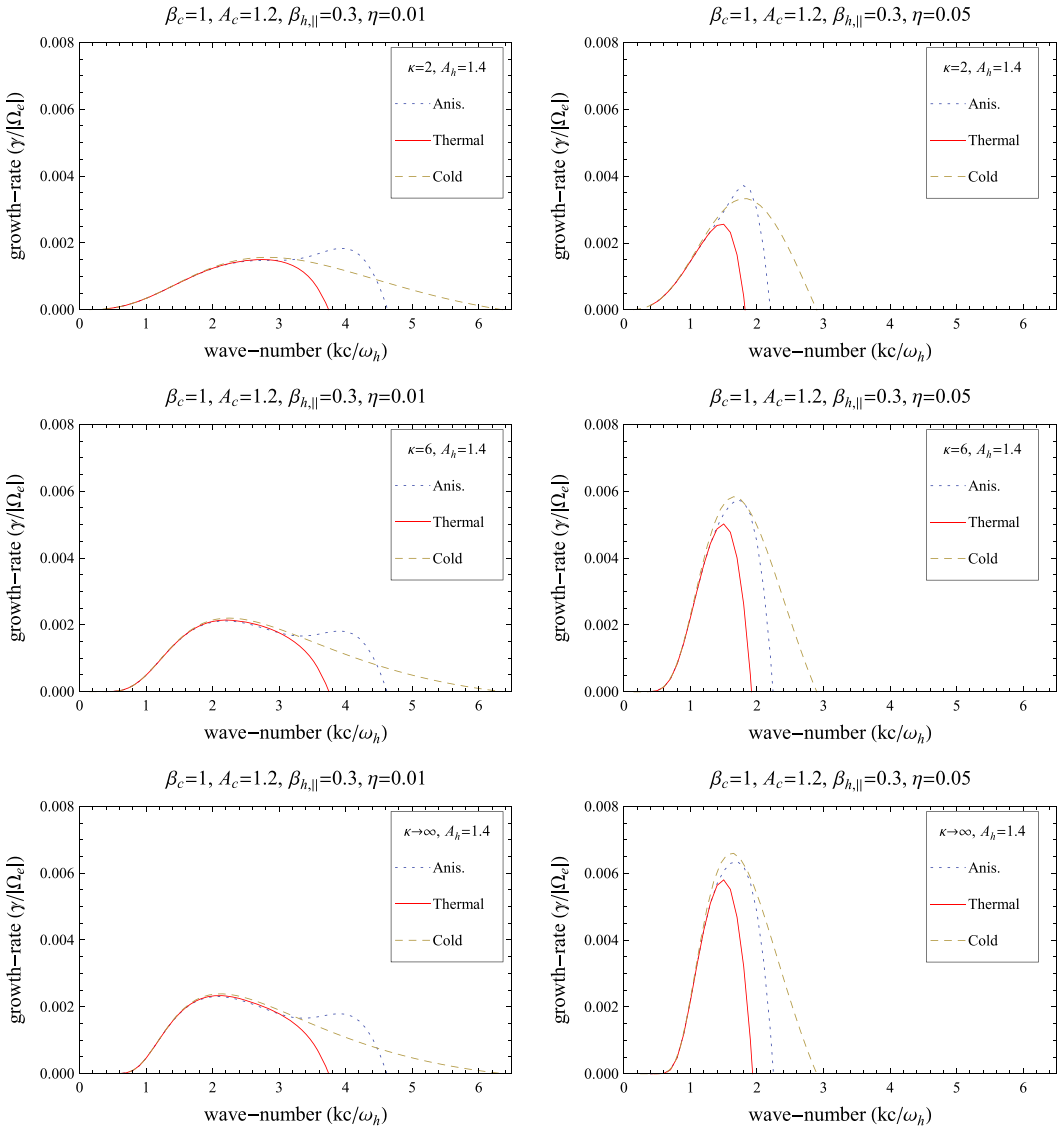

Figure 6. The same as in Figure 5 but for a higher $\beta_{h,\|} = 0.3$.

anisotropic with $T_{c,\perp} > T_{c,\|}$ and $T_{h,\perp} > T_{h,\|}$, respectively (dotted lines); (ii) the case studied by *Lazar et al.* [2015] when the core is isotropic $T_{c,\perp} = T_{c,\|}$, and $T_{h,\perp} > T_{h,\|}$ (solid lines); and (iii) the idealized case when the core is taken cold and $T_{h,\perp} > T_{h,\|}$ (dashed lines). For the last two cases, in the plots, we keep the line styles used by *Lazar et al.* [2015]. In the same paper the range of halo beta values $0.05 \leqslant \beta_h \leqslant 1$ was found relevant for a selection of slow wind events, and here this interval is marked with gray shading. A comparison is also made for different Kappa models, e.g., top for $\kappa = 2$, middle for $\kappa = 6$, and bottom for the limit case $\kappa \to \infty$ when both the core and halo populations are modeled by Maxwellian distribution functions (two-Maxwellian model).

The anisotropy thresholds decrease with increasing plasma beta because hotter halo populations need lower anisotropies to ignite the instability. In the presence of a temperature anisotropy in the core, the thresholds are lowered, indicating that the instability is enhanced. This effect is more pronounced at lower thresholds, e.g., $\gamma_m/\Omega = 10^{-3}$ (lower anisotropies in the halo), which drop below those provided by the cold-core-based model. Moreover, the effect of the core anisotropy becomes important, showing large deviations from the previous models, whenever we reduce the influence of the halo, for instance, when the halo beta is decreased. When the instability is triggered by both the core and halo populations, the influence of the last on the instability thresholds is less significant, but it follows the same trend of

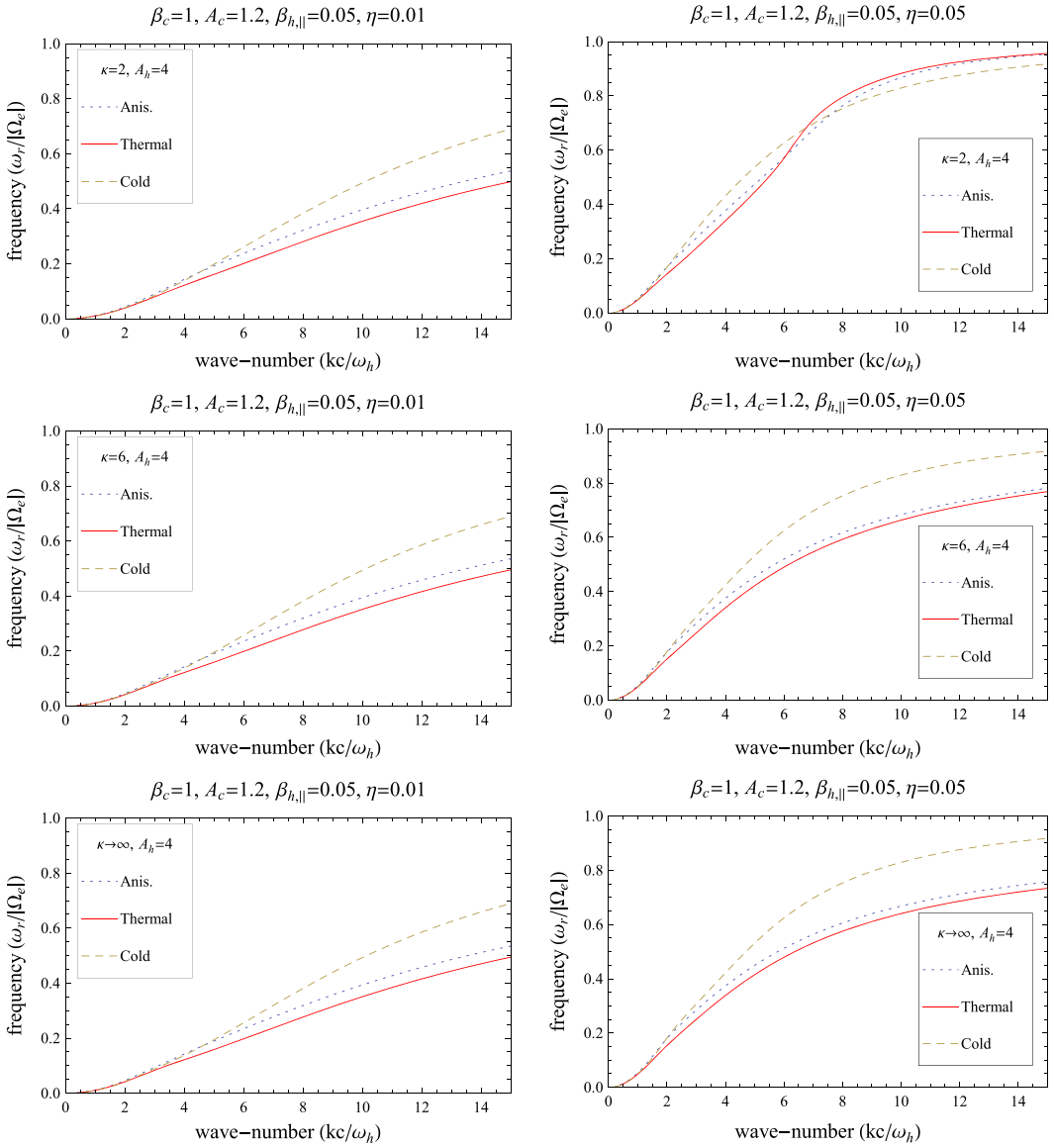

Figure 7. Frequency of the unstable modes in Figure 5.

variation. Thus, an increase of the relative (halo-core) density η from 0.01 to 0.05 inhibits the instability at low betas ($\beta_{h,\|} \leqslant 0.05$), but it can enhance the instability at higher betas. On the other hand, the influence of suprathermal populations from the halo is more uniform, the instability thresholds being increased with decreasing the power index $\kappa \to 2$.

3.2. Unstable Solutions

The unstable solutions are derived for different values of the halo beta parameter $\beta_{h,\|}$ and the halo-core relative density η. At low values of the halo beta, e.g., $\beta_{h,\|} = 0.05$ (Figure 5), the instability is inhibited by increasing the relative density from $\eta = 0.01$ (Figure 5, left) to $\eta = 0.05$ (Figure 5, right), while for large halo betas, e.g., $\beta_{h,\|} = 0.3$ (Figure 6), the instability is stimulated by increasing the growth rates with increasing the relative density. With increasing η, the range of the unstable wave numbers is always restrained to lower values.

Noticeable are the growth rates with two distinct peaks (see Figure 6), one driven by the halo anisotropy at low wave numbers and the second one driven by the core anisotropy at higher wave numbers. According to the resonance condition $|f| \sim 1$ (or $|f_\kappa| \sim 1$), the less energetic electrons resonate with modes of higher wave numbers. Growth rates with two peaks are, in general, obtained when the halo anisotropy is

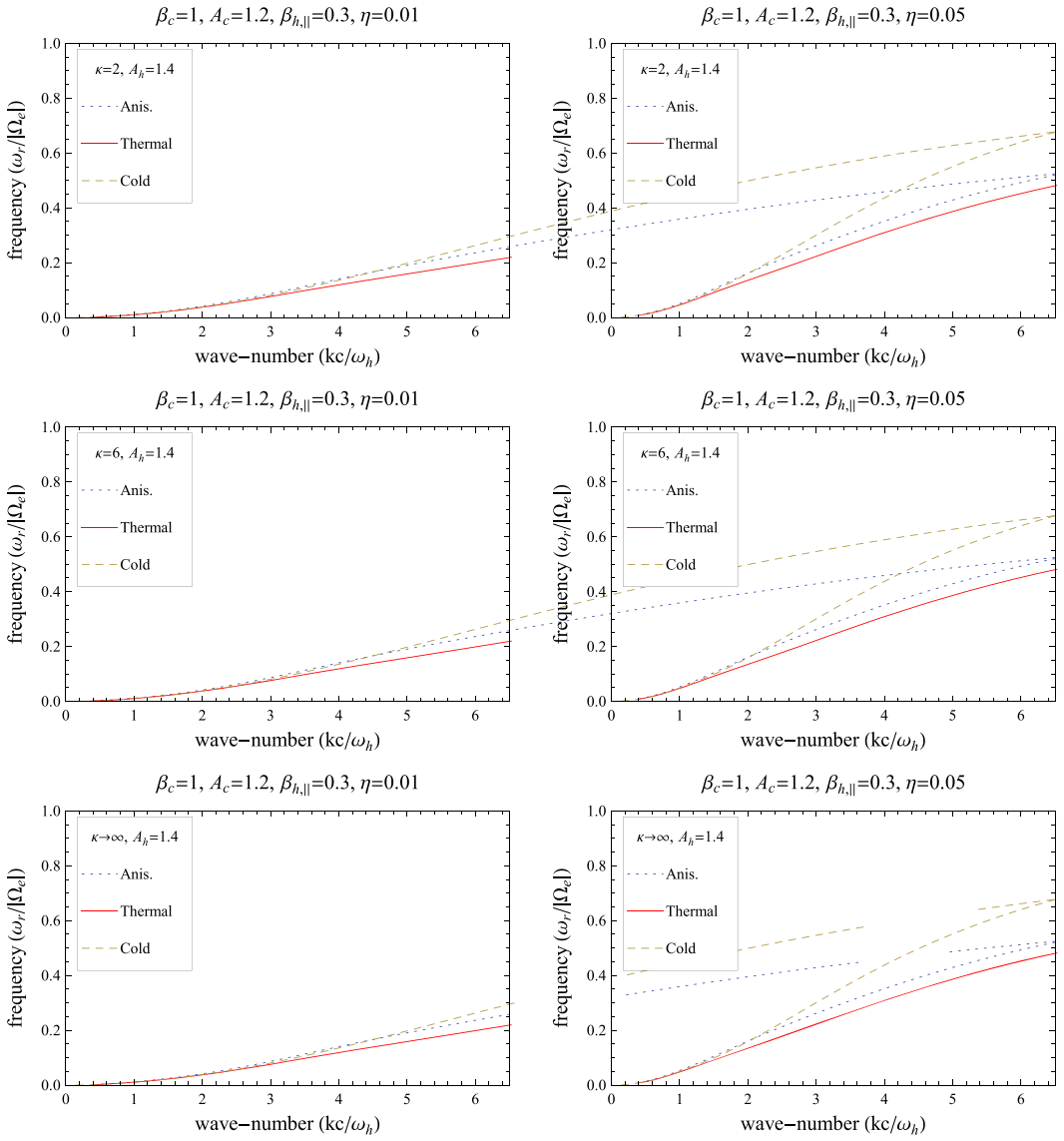

Figure 8. Frequency of the unstable modes in Figure 6.

comparable with that observed in the core. However, the first peak is inhibited by the presence of suprathermal populations (lowering $\kappa \to 2$), while the second peak is sustained, exceeding the first peak and suggesting a more intricate connection between the core and halo populations.

Corresponding to the growth rates in Figures 5 and 6, the wave frequency is displayed in Figures 7 and 8, respectively. As for the growth rates, the differences between our models become significant at higher wave numbers. The wave frequency predicted by the model with an anisotropic core is always placed between frequencies predicted by the other two models.

In Figure 9 we show what happens with the growth rates when the core anisotropy is slightly increased to $A_c = 2$. Only the cases of low $\beta_{h,\|} = 0.05$ are displayed here since the effects are reproducible for higher values of this parameter. The instability is markedly stimulated by increasing the core anisotropy. Thus, a comparison with Figure 5 reveals that just a modest increase from $A_c = 1.2$ to $A_c = 2$ causes the growth rate to increase by 1 order of magnitude and the range of unstable wave numbers to extend considerably.

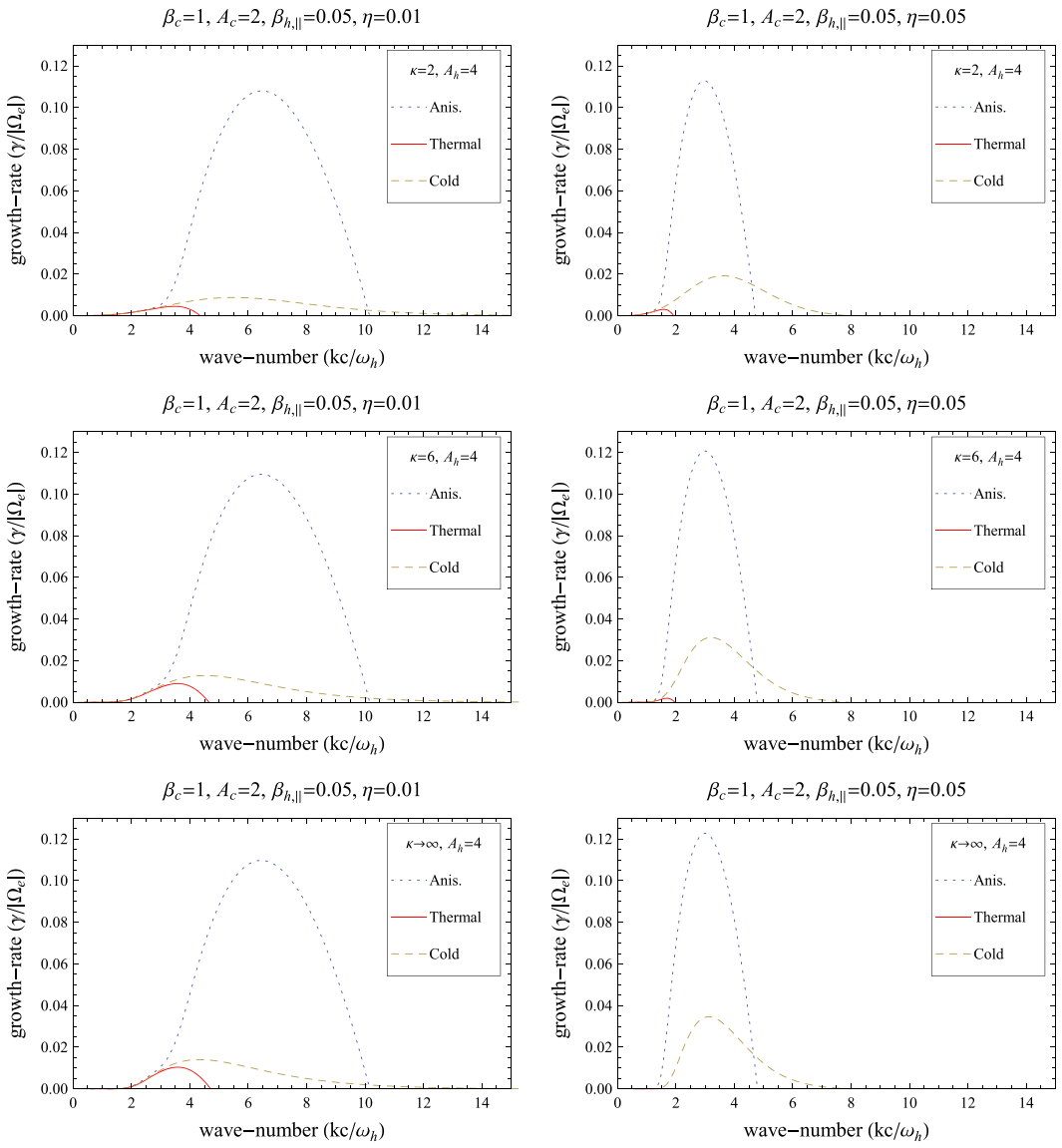

Figure 9. The same as in Figure 5 but for a higher anisotropy in the core $A_c = 2$.

4. Summary and Conclusions

Realistic models of VDFs facilitate accurate descriptions of the kinetic plasma instabilities and the role played by the resulting fluctuations in the solar wind and planetary magnetospheres. In the present paper we have shown how to improve the ability to parameterize and predict the space plasma dynamics, especially for nonidealized situations when both the core and halo temperatures are finite and anisotropic. An extended comparison with the previous approaches where the core was assumed isotropic or even cold enabled us to describe the interplay between these two components, namely, the Maxwellian core and the Kappa halo.

To point out the main effects of this interplay here, we have analyzed the EMEC instability. This instability is considerably stimulated when both the core and halo populations are anisotropic. The instability thresholds as well as growth rates show important departures from the previous models which assume the core cold or isotropic. The wave numbers stabilized by an isotropic core become unstable even for small anisotropies of this component. When the core and halo anisotropies are comparable, the growth rate exhibits two peaks, one driven by the halo anisotropy at low wave numbers and another one driven by the core anisotropy at higher wave numbers. The first peak is found to be inhibited by the suprathermal populations in accord

with the previous studies [*Lazar et al.*, 2011], where this effect has been shown the first time but for a global Kappa model. At the same time, if the relative halo-core density is sufficiently low, the second peak (driven by the core) appears to be enhanced by the suprathermals, suggesting a more intricate connection between these components.

Future studies may consider the same formalism to characterize other instabilities, e.g., firehose or mirror instability, of interest in space plasma physics. Even for situations when the core and halo populations are (nearly) isotropic, the simple contrast between these components can be a source of free energy and plasma instabilities in the presence of finite Larmor radius effects [*Pokhotelov et al.*, 2005]. Moreover, the two-component model has also been found relevant for the ion distributions observed in space plasmas [*Christon et al.*, 1988, 1991; *Collier et al.*, 1996]. To investigate the instabilities driven by the anisotropic ions, the same models of VDFs proposed here in equations (1)–(7) can be invoked.

Acknowledgments

Thanks are due to Jens Pomoell for support in processing the observational data. The authors acknowledge use of the *Ulysses*/SWOOPS electron data from the ESA-RSSD Web service ftp://www.rssd.esa.int/pub/ulysses/data/swoops/ and *Ulysses* 1 h averaged measurements of magnetic field and solar wind bulk speed data ftp://spdf.gsfc.nasa.gov/pub/data/ulysses/merged/. The authors acknowledge support from the Katholieke Universiteit Leuven grant SF/12/003 and from the Ruhr-Universität Bochum, and the Deutsche Forschungsgemeinschaft (DFG) grant Schl 201/25-1. These results were obtained in the framework of the projects GOA/2015-014 (KU Leuven), G.0729.11 (FWO-Vlaanderen), and C 90347 (ESA Prodex 9). The research leading to these results has also received funding from the European Commission's Seventh Framework Programme (FP7/2007-2013) under the grant agreements SOLSPANET (project n 269299, www.solspanet.eu), and eHeroes (project 284461, www.eheroes.eu).

Yuming Wang thanks the reviewers for their assistance in evaluating this paper.

References

Bale, S. D., J. C. Kasper, G. G. Howes, E. Quataert, C. Salem, and D. Sundkvist (2009), Magnetic fluctuation power near proton temperature anisotropy instability thresholds in the solar wind, *Phys. Rev. Lett.*, *103*, 211101.

Christon, S. P., D. G. Mitchell, D. J. Williams, L. A. Frank, C. Y. Huang, and T. E. Eastman (1988), Energy spectra of plasma sheet ions and electrons from ∼ 50 eV/*e* to ∼1 MeV during plasma temperatures transitions, *J. Geophys. Res.*, *93*, 2562–2572.

Christon, S. P., D. J. Williams, D. G. Mitchell, C. Y. Huang, and L. A. Frank (1991), Spectral characteristics of plasma sheet ion and electron populations during disturbed geomagnetic conditions, *J. Geophys. Res.*, *96*, 1–22.

Collier, M. R., D. C. Hamilton, G. Gloeckler, P. Bochsler, and R. B. Sheldon (1996), Neon-20, Oxygen-16, and Helium-4 densities, temperatures, and suprathermal tails in the solar wind determined with WIND/MASS, *Geophys. Res. Lett.*, *23*, 1191–1194.

Fried, B. D., and S. D. Conte (1961), *The Plasma Dispersion Function*, Academic Press, New York.

Kennel, C. F., and H. E. Petschek (1966), Limit on stably trapped particle fluxes, *J. Geophys. Res.*, *71*, 1–28.

Lazar, M., R. Schlickeiser, and P. K. Shukla (2008), Cumulative effect of the Weibel-type instabilities in symmetric counterstreaming plasmas with kappa anisotropies, *Phys. Plasmas*, *15*, 042103.

Lazar, M., S. Poedts, and R. Schlickeiser (2011), Instability of the parallel electromagnetic modes in Kappa distributed plasmas—I. Electron whistler-cyclotron modes, *MNRAS*, *410*, 663–670.

Lazar, M., S. Poedts, R. Schlickeiser, and C. Dumitrache (2015), Towards realistic parameterization of the kinetic anisotropy and the resulting instabilities in space plasmas. Electromagnetic electron cyclotron instability in the solar wind, *MNRAS*, *446*, 3022–3033.

Maksimovic, M., et al. (2005), Radial evolution of the electron distribution functions in the fast solar wind between 0.3 and 1.5 AU, *J. Geophys. Res.*, *110*, A09104, doi:10.1029/2005JA011119.

Marsch, E. (2006), Kinetic physics of the solar corona and solar wind, *Living Rev. Sol. Phys.*, *3*, 1. [Available at http://www.livingreviews.org/lrsp-2006-1.]

Pierrard, V., and M. Lazar (2010), Kappa distributions: Theory and applications in space plasmas, *Sol. Phys.*, *267*, 153–174.

Pokhotelov, O. A., M. A. Balikhin, R. Z. Sagdeev, and R. A. Treumann (2005), Halo and mirror instabilities in the presence of finite Larmor radius effects, *J. Geophys. Res.*, *110*, A10206, doi:10.1029/2004JA010933.

Stverak, S., P. Travnicek, M. Maksimovic, E. Marsch, A. N. Fazakerley, and E. E. Scime (2008), Electron temperature anisotropy constraints in the solar wind, *J. Geophys. Res.*, *113*, A03103, doi:10.1029/2007JA012733.

Scudder, J. D., and S. Olbert (1979), A theory of local and global processes which affect solar wind electrons: 1. The origin of typical 1 AU velocity distribution functions—Steady state theory, *J. Geophys. Res.*, *84*, 2755–2772.

Vasyliunas, V. M. (1968), A survey of low-energy electrons in the evening sector of the magnetosphere with OGO 1 and OGO 3, *J. Geophys. Res.*, *73*, 2839–2884.